# Optimization of Exciton-Induced Detection of Atoms at Interfaces†

**M. Dickgiesser and N. Schwentner***

*Institut für Experimentalphysik, Freie Universität Berlin, Arnimallee 14, D-14195 Berlin, Germany*

*Received: November 2, 1999; In Final Form: January 31, 2000*

By modeling diffusion-controlled exciton energy transfer to atoms at the interface or surface of rare gas films it is shown that about 10% of the available light flux can be funneled to a coverage of the order of 1/100 of a monolayer. Analytical expressions for the transfer efficiency with respect to absorption coefficient, diffusion length, boundary condition, and the linear range of detection probability are presented and applied to F atoms in a Kr/Ar interface. Transfer efficiencies, exciton diffusion lengths and densities are derived from the measured spectral and thickness dependences of the $Kr_2$* and $Kr_2F$ fluorescence. This system provides nearly optimal parameters, and the potential for penetration depth measurements of atoms is illustrated.

## Introduction

The model character of excitonic excitations in rare gas solids with respect to the energetic structure, energy transport, and electron−phonon interaction causing self-trapping is documented in several reviews.[1−3] More insight into the relaxation dynamics[4] and into exciton-induced desorption processes[5,6] was obtained in the meantime from experimental and theoretical investigations. The interesting competition between delocalization by free exciton migration and localization by self-trapping motivated several studies on energy transport to statistically distributed dopands,[2,7] to condensates on surfaces with enhanced quenching,[8] and to metal substrates resulting in electron ejection.[9] Diffusion lengths for the especially well investigated Kr excitons of the order of 10 to 1000 nm were determined, and a systematic increase with exciton energy[7,9] and with the structural quality of the Kr films was observed.[7] Doped rare gas films play a key role in another area of research which is matrix isolation spectroscopy for photochemical applications. This field was pioneered by Marilyn E. Jacox. She started also the investigations of reactions of F atoms in matrices,[10−13] and the transport of F atoms to reaction partners is the central topic of this contribution. The fragment migration in the bulk has an interesting counterpart in desorption studies with the ejection of atoms from subsurface layers.[14] The microscopic description of these elementary photoreactions, which involve photodissociation of a small molecule, cage exit and migration of a fragment, and finally formation of a new band, has reached a rather high level of sophistication in experiment and theory.[15,16] A new type of experiment was introduced to measure directly the penetration depths of atoms with several eV of kinetic energy in rare gas films.[17,18] In a sandwich of three rare gas films, hot atoms from photodissociaton are ejected from a surface layer, penetrate through a spacer layer of variable thickness, and that fraction of atoms which reaches the interface to a substrate layer is recorded. The method was successfully applied, and penetration depths of about 10 monolayers for F atoms with 4.3 eV kinetic energy were determined for Ar spacer layers in photodissociating $F_2$ molecules in the top layer and detecting the F atoms in the interface to a Kr substrate layer. The penetration depths were discussed with respect to the mean free path and the energy loss per collision, and they were compared with the molecular dynamics calculations and with results from statistically doped samples.[16,18]

Paramount for the method is a high sensitivity in the detection of the atoms at the interface. A remarkably high sensitivity of the order of 1/1000 of a monolayer was reached by exciting the interface atoms with excitons created in the substrate. The efficiency of the exciton-induced excitation exceeds that for direct excitation with light by several orders of magnitude.[18] The enhanced sensitivity by exciton energy transfer to the interface atoms is crucial for the applicability of the method; nevertheless, the energy transfer processes were not yet modeled or treated quantitatively. Therefore, these processes are studied in detail in this contribution. The fluorescence intensities of the self-trapped excitons in the substrate and of the atoms at the interface are used to monitor the exciton densities and the transfer efficiency, respectively. A high exciton density at the interface enhances the transfer efficiency, and its dependence on the light penetration depth follows from scanning through the spectrum of the substrate excitons. The boundary conditions with respect to exciton quenching or reflection are especially important at this interface. They are derived from the spectral and thickness dependence of the emission intensities together with the diffusion length of the excitons. The modeling is based on experience from the previous exciton transport studies[7−9] with special emphasis on the conflicting boundary conditions. General criteria on how to optimize the transfer efficiency are derived. In addition, it is discussed in which way the transfer efficiency can be monitored by the substrate emission, and a significant improvement in the scatter of measured penetration probabilities is demonstrated. The study deals with Kr substrates because of the available optical constants, the extensive previous studies on exciton migration, and the favorable energetics for the F atom detection. The results can be generalized to any combination of rare gas films and atoms or molecules in interfaces. Surfaces are a special type of interface and therefore the contributions of bulk excitations to the desorption on rare gas surfaces[19] can be modeled in a similar way.

† Part of the special issue "Marilyn Jacox Festschrift".

* Corresponding author. Telephone +49 30 838 6035. Fax +49 30 838 3050. E-mail Nikolaus.Schwentner@physik.fu-berlin.de

10.1021/jp9938821 CCC: $19.00 
Published on Web 03/18/2000

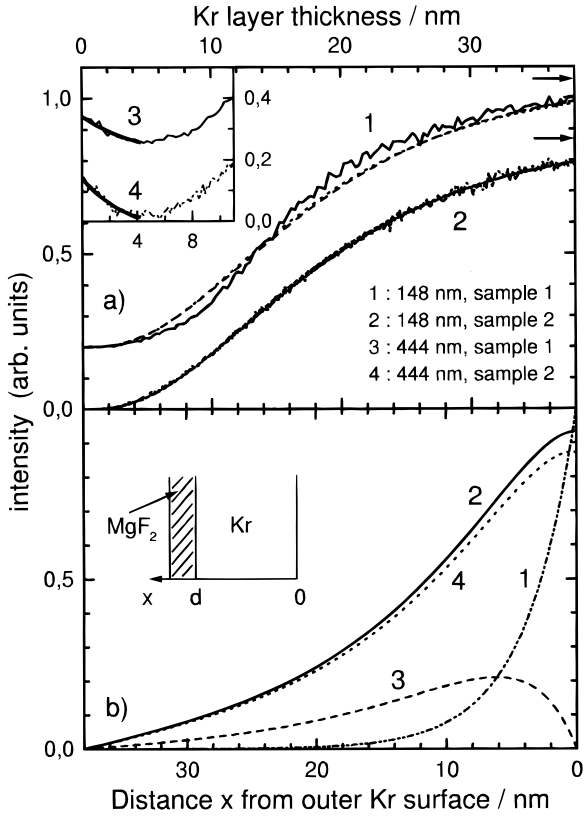


**Figure 1.** (a) Growth of $Kr_2$* emission (148 nm) with layer thickness on $MgF_2$ substrate for excitation in $n = 1$ exciton (10.15 eV). Sample 1 intensity (curve 1) exceeds sample 2 intensity (curve 2) by a factor of 1.3. The fits with bc1 (eq 4) and bc2 (eq 5) to curve 1 (dashed lines) and curve 2 (solid lines) are indistinguishable, and arrows give saturation value. Inset shows corresponding decay of substrate emission at 444 nm for sample 1 (curve 3) and sample 2 (curve 4) together with fits using $\mu = 0.21$ nm$^{-1}$ and 0.28 nm$^{-1}$, respectively. (b) Absorption profile with $\mu = 0.25$ nm$^{-1}$ in $n = 1$ exciton (curve 1) and spatial exciton density profiles $n(x)$ with bc2 (eq 5, curve 2), with bc1 (eq 4, curve 3), and bc3 (eq 6, curve 4) for quenching of $n(0)$ by 7%. For details see text.

## Experimental Section

Sandwich-like samples were grown on a cooled $MgF_2$ substrate in ultrahigh vacuum at a background pressure below $10^{-8}$ mbar. Typically, a Kr film of 40 nm thickness was covered with a pure Ar spacer layer of variable thickness $d$, and the sample was completed with a 5 nm thick Ar layer doped with 0.5 atm % $F_2$. Three independent gas handling systems and three deposition tubes were used to avoid intermixing, and the thicknesses were controlled by a combination of quartz microbalance and optical interference fringes with monolayer accuracy as described in ref 18. The Ar spacer layer was omitted ($d_{Ar} = 0$) in the samples presented in Figures 1 to 4 because the central topic of this contribution is the energy transfer from the Kr layer to F atoms at the Kr/Ar interface. Results for the transport through the spacer layer ($d_{Ar} \neq 0$) are collected in Figure 5. A compromise was necessary concerning deposition temperature $T_d$ and deposition rate $k_d$ to avoid intermixing (low $T_d$), to ensure complete coverage of the Kr film by a compact Ar film (high $T_d$, low $k_d$), and to reduce the intake of impurities from the residual gas (high $k_d$). Values of $T_d = 5$ K and $k_d = 0.5$ monolayers per second were chosen. The compactness of the Ar and $F_2$/Ar films was checked via the intensity decrease of the Kr surface excitons, and only samples with a quenching by at least a factor of 10 were accepted.[18]

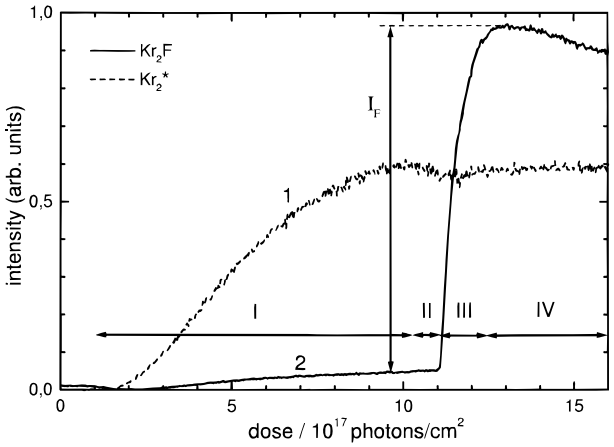


**Figure 2.** Irradiation history of sample 2 with region I: growth of Kr film to 38 nm thickness, region II: 50 s switching time, region III: growth of 5 nm film 0.5% $F_2$ in Ar, region IV: prolonged irradiation. Curve 1: $Kr_2$* intensity (148 nm), curve 2: $Kr_2F$ intensity (444 nm) for continuous irradiation in $n = 1$ exciton (10.15 eV). $I_F$ corresponds to $Kr_2F$ intensity used in Figure 5.

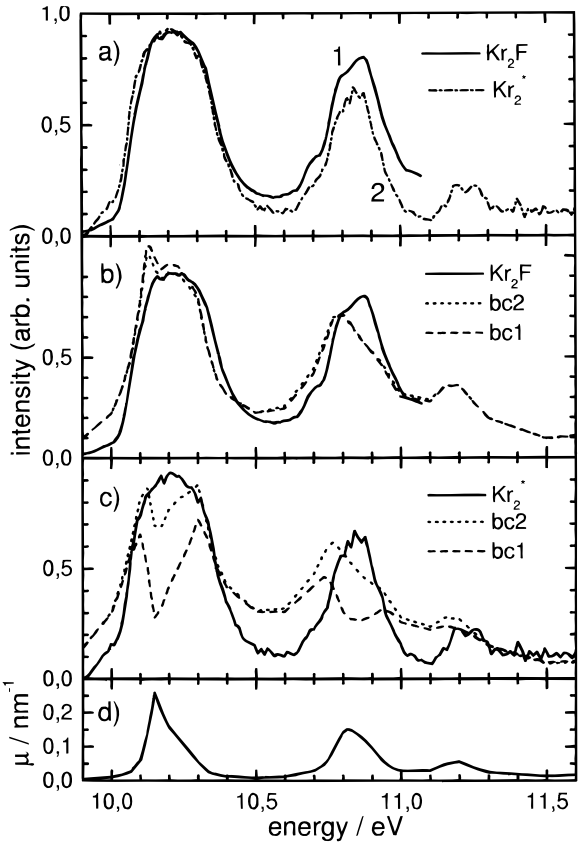


**Figure 3.** (a) $Kr_2F$ (444 nm) and $Kr_2$* (148 nm) emission intensity versus excitation energy in the $n = 1$ to $n = 2$ exciton regime normalized to maximal values. (b) Comparison of $Kr_2F$ intensity with fits using bc1 (dashed line) and bc2 (dotted line), fit parameters see Table 1. (c) As (b) for $Kr_2$* intensity. (d) absorption coefficient from ref 21.

The samples were excited with wavelength-dispersed synchrotron radiation in our matrix setup at BESSY I[20] in the spectral range from 150 to 100 nm with special emphasis on the range of the Kr excitons up to the band gap energy. The fluorescence intensity of the molecular type self-trapped Kr excitons $Kr_2$* at 148 nm (ref 2) and the fluorescence of a dopand, typically that of $Kr_2F$ at 444 nm, were recorded

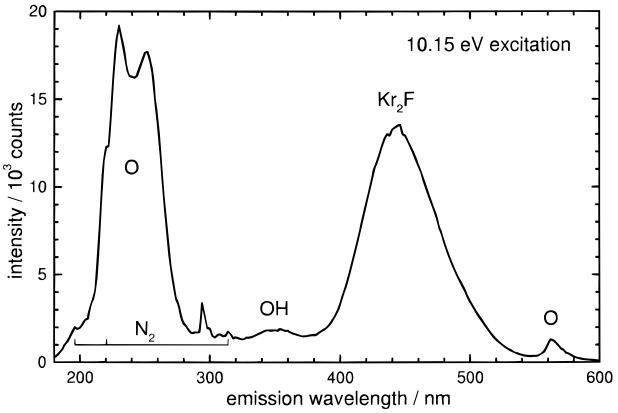


**Figure 4.** UV and visible emission spectrum of sample 1 for excitation at 10.15 eV with bands due to $Kr_2F$, OH, $N_2$, and O.

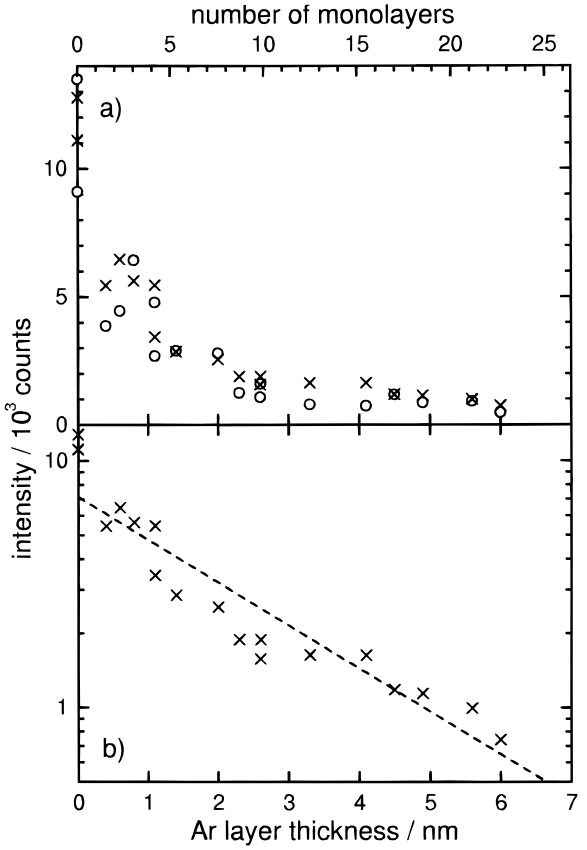


**Figure 5.** (a) $Kr_2F$ emission intensity (444 nm) of F atoms at Kr/Ar interface versus thickness of Ar spacer layer (circles) and the same values normalized to $Kr_2$* intensity (crosses) for excitation at 10.15 eV. (b) Normalized values on logarithmic scale with linear regression (dashed line) for F atom penetration depth of 2.5 nm (9 monolayers).

simultaneously via two independent monochromators and detection lines.[18] The variation of the fluorescence intensity with the excitation wavelength represents an excitation spectrum, and these spectra (Figure 3) are corrected for the wavelength dependence of the incoming photon flux which amounts to $5 \times 10^{14}$ photons/s/cm$^2$ at 10 eV.

## Results

The main aim of this study is an optimization of the detection sensitivity for atoms, especially F atoms, at the Kr/Ar interface. Exciton energy transfer enhances the sensitivity by orders of magnitude compared to light absorption in the atoms.[18] Therefore, we want to determine the spatial distribution of the excitons in the Kr film and to characterize the transfer process itself. This information will be used to derive a recipe for the highest sensitivity. The efficiency will scale with the amount of excitons. By measuring this quantity in each sample we will investigate to which extent the scatter in the data for F atom concentrations at the Kr/Ar interface versus spacer thickness originates from unintentional sample-to-sample variations of the exciton concentration and thus can be reduced. The atoms under investigation are located at the Kr/Ar interface, and the generation of Kr excitons close to this interface will support the transfer efficiency. Therefore, irradiation from the front side (outer Kr surface) with a photon energy just in the center of the $n = 1$ exciton band of Kr (10.15 eV) which provides the highest absorption coefficient should be favorable. The $Kr_2$* fluorescence intensity is used to monitor the overall amount of Kr excitons which survive quenching at the outer and inner interface (i.e., the Kr/Ar and $MgF_2$/Kr interface, respectively). The increase of this emission with Kr film thickness for irradiation at 10.15 eV is shown in Figure 1a for two typical samples together with the emission intensity from the $MgF_2$ substrate (inset, curves 3 and 4) recorded at 444 nm emission wavelength. The emission shown in the inset is already present for the bare $MgF_2$ substrate without the Kr layer, and therefore it does not arise from $Kr_2F$ centers. We assign it to color centers formed inside the $MgF_2$ substrate leading to a broad emission centered around 320 nm with a red wing extending beyond the wavelength of 444 nm used for detection. The increasing absorption in the Kr film blocks the light for the substrate, and the substrate emission decays quickly according to the known Kr absorption coefficient $\mu = 0.25$ nm$^{-1}$ [21] (corresponding to a light penetration depth $l_0 = 4$ nm) and reaches a minimum around 5 nm Kr film thickness. The rise of the $Kr_2$* intensity with thickness in Figure 1a is delayed compared to the decay in the inset. At a film thickness of 5 nm, only 5% of the final value around 38 nm is reached, which is close to the saturation value indicated by an arrow.

This delay will be attributed in the discussion to exciton diffusion characterized by a diffusion length $l$ and to quenching processes which can occur on the inner and outer surface of the Kr film. Exciton diffusion will be responsible also for the intended energy transfer to the interface atoms, and its quantitative description is essential for optimization of the detection efficiency. The thickness of about 20 nm necessary to reach the $1-1/e$ value in Figure 1a indicates in a qualitative way that indeed quenching at one or both interfaces is severe, causing a quenching range of more than 10 nm. Thus $l$ will be around 10 nm and it exceeds $l_0$ considerably. The two samples in Figure 1a differ in the saturated $Kr_2$* intensity; sample 1 provides a factor of 1.3 higher intensity at 38 nm thickness than sample 2. For comparison of the rising part the intensities are normalized to equal values at 38 nm and shifted vertically for clarity. Figure 1b shows the absorption profile of the final film determined by $l_0$ (curve 1) and the spatial exciton distributions $n(x)$ from the modeling in the discussion section (curves 2, 3, and 4). The rise of the fluorescence intensity at 444 nm beyond 5 nm thickness (inset 1a, curves 3 and 4) follows that of the $Kr_2$* emission and belongs to an unspecified emission from the film.

The complete preparation and irradiation history of sample 2 in Figure 1a is displayed in Figure 2. The region I extending to a dose of $10 \times 10^{17}$ photons/cm$^2$ corresponds to the growth of the Kr film up to 38 nm thickness as shown also in Figure 1a, and curve 1 is the $Kr_2$* intensity and curve 2 the emission at 444 nm. The sample was exposed to residual gas in region II

for a time interval of 50 s which was required to close and open the gas lines. A 5 nm thick $F_2$/Ar layer is condensed in region III. The sample is irradiated all the time with 10.15 eV photons. The $F_2$ content is dissociated, and F atoms accumulate at the Kr/Ar interface. The $Kr_2F$ emission specific for F atoms at this interface peaks at 444 nm, [18] and the rise of curve 2 in region III displays the increasing F content at the interface. The preparation is finished at the end of region III, and in region IV the sample is exposed further to light. A small fraction of $F_2$ molecules is condensed in the beginning of region III at the interface since no Ar spacer layer is used in this sample. This fraction contributes to the $Kr_2F$ band via a light-induced harpooning reaction. $(KrF_2)^* \rightarrow KrF^* + F$ in this reaction, and KrF* forms $(Kr_2F)^*$ which radiates. The $F_2$ fraction is decomposed in this process, and the weak decay in region IV reflects this contribution.[18] The intensity increase $I_F$ above the background will be used in the following to monitor the excitation efficiency of F atoms.

The $Kr_2^*$ intensity remains essentially constant in region II, which indicates only a weak quenching by energy transfer to residual gas accumulated in this period on the surface. From region I to region III a decrease by about 5% is observed and it indicates a loss of excitons due to energy transfer to the F atoms, which is the intended process.

The absorption coefficient of Kr determines the generated exciton density near the Kr/Ar interface. Thus this density can be systematically reduced by scanning through the wings of the $n = 1$ exciton absorption band. The energy transfer efficiency monitored by the $Kr_2F$ intensity (Figure 3a, curve 1) indeed decreases with the absorption coefficient $\mu$ (Figure 3d) taken from the literature.[21] The $Kr_2^*$ intensity should reflect the exciton density integrated over the sample thickness which will also decrease in the wing. Indeed the $Kr_2^*$ intensity (Figure 3a, curve 2) shows the expected trend. Nevertheless, the very close similarity in the shapes of the excitation bands of $Kr_2^*$ and $Kr_2F$ are not immediately obvious since the former corresponds to the integral while the latter follows the density of excitons near the interface. This similarity will be a crucial test for the modeling. The close correspondence of the excitation line shape for both emissions and with the absorption band shape is also observed for the $n' = 1$ exciton around 10.85 eV. But comparing $n = 1$ and $n' = 1$, it is obvious that for similar $\mu$ values in both excitons the $Kr_2^*$ as well as the $Kr_2F$ intensities differ, which is a signature of the known increase of the diffusion length with exciton energy.[7,9]

The emission spectrum of the molecular self-trapped excitons at 148 nm is identical with the literature data[2] and not reproduced. The emission spectrum of a complete sample with $F_2$/Ar top layer in the region from 200 to 600 nm (Figure 4) contains the strong $Kr_2F$ emission centered at 444 nm which was analyzed in detail[18] and is assigned to F atoms at the Kr/Ar interface.

The strong and split band around 250 nm and the weak band at 563 nm result from an unintentional atomic oxygen impurity. The high energetic emissions were attributed to KrO Rydberg or ionic transitions,[22] and the long wavelength band is the well-known $^1S \rightarrow {}^1D$ transition of O.[23] The atomic oxygen results presumably from dissociation of $O_2$ and $H_2O$ impurities accumulated from impurities in the gases themselves, in the gas lines, and the residual gas. The O intensity varies from sample to sample and is not correlated to the $Kr_2^*$ intensity or the $Kr_2F$ intensity. Therefore, the energy transfer to F atoms is not influenced in an obvious competitive way by the O content. The broad band around 370 nm corresponds at least partly to OH[24,25] from the dissociation of $H_2O$. Some weak features between 200 and 300 nm result from the $X \leftarrow A^3\Sigma$ emission of $N_2$.[26] The sharp band at 295 nm is always present with varying intensity and not yet identified. It has to be pointed out that we use gases of high purity (Kr: 99.998%, Ar: 99.9999%). The gas handling system and the sample chamber are kept in ultrahigh vacuum conditions. The weakness of contamination by residual gas for example is evident from the strong contribution of surface excitons which would already be quenched by a monolayer of impurities but which is stable for hours.[18] A likely source of impurities is the substrate which is exposed to the residual gas in all cooling cycles. An accumulated impurity layer between the $MgF_2$ substrate and the Kr film would be exposed to the excitons, and mobile dissociation products such as O atoms[27] may even penetrate into the Kr film. The excitation scheme via excitons provides a sensitivity even for 1/1000 of a monolayer, and therefore spurious contaminations may show up in such strong emission features. Figure 4 illustrates the flexibility of the sandwich method also for other dopands as F atoms and especially oxygen seem to be promising candidates for future studies.

Finally a good correlation was observed in the Ar spacer-free samples between the $Kr_2^*$ and the $Kr_2F$ emission intensity for excitation at 10.15 eV. This observation provides an empirical basis to correlate the sensitivity for F atom detection with the amount of excitons via the $Kr_2^*$ intensity. To prove and exploit this calibration of the sensitivity for each individual sample, a large set of 20 sandwich samples was prepared with Ar spacer layers varying from few monolayers up to 6 nm (20 monolayers). All samples were treated similar to that in Figure 2, and the $Kr_2F$ intensity ($I_F$) versus Ar spacer layer thickness is plotted in Figure 5a by open circles. The expected trend of a decreasing intensity with spacer thickness due to the reduced probability that the F atoms penetrate through the layer is observed, but the scatter of the data is considerable. For each sample also the $Kr_2F/Kr_2^*$ ratio is reproduced in Figure 5a and 5b by crosses (in arb. units) and it is immediately evident that the scatter is significantly reduced. This correction amounts in several cases to a factor of 2 and is obviously relevant to derive reliable values for the penetration depth of the F atoms.

## Discussion

The spatial distribution $n(x)$ of the excitons in the Kr films is central in the discussion. Its connection to an exciton diffusion equation was established especially for Kr films already in ref 8 and confirmed later on.[7,9] Using the notation of the recent publication,[7] the exciton diffusion can be modeled by means of three differential equations:

$$\frac{dn}{dt} = I_0(1-R)\mu e^{-\mu x} + D\frac{d^2n}{dx^2} - \frac{n}{\tau_0} - Sn(c_0 - c_e) \quad (1a)$$

$$\frac{dc_e}{dt} = Sn(c_0 - c_e) - \frac{c_e}{\tau_c} \quad (1b)$$

$$\frac{dn_{ST}}{dt} = n\left(\frac{1}{\tau_0} - \frac{1}{\tau_r}\right) - \frac{n_{ST}}{\tau_{ST}} \quad (1c)$$

with $n(x,t)$, free-exciton density at time $t$ and at distance $x$ from the outer surface; $I_0$, number of incident photons per area and time; $\mu$(E), absorption coefficient; $R$(E), reflectivity; $D$, diffusion constant; $\tau_0$, lifetime of free excitons with respect to self-trapping and direct recombination; $S$, trapping rate of the trapping centers; $c_0$, trapping center concentration; $c_e$, concentration of excited

trapping centers; $\tau_c$, lifetime of the excited state of the trapping centers; $n_{ST}$, density of the self-trapped excitons; $\tau_{ST}$, radiative lifetime of self-trapped excitons; and $\tau_r$, radiative lifetime of free excitons.

These equations can be simplified assuming $1/\tau_0 \gg 1/\tau_r$ and $c_0 \gg c_e$ together with the introduction of an effective lifetime $\tau$ of the excitons which may also contain, in addition to the self-trapping time $\tau_0$, a contribution from quenching by homogeneously distributed impurities in the film with concentration $c_0$ and trapping rate $S$:

$$\frac{1}{\tau} = \frac{1}{\tau_0} + Sc_0 \tag{2}$$

The intensity $I_{STE}$ of the self-trapped exciton emission $Kr_2$* is obtained from integration of the spatial distribution $n(x)$ up to the film thickness $d$ for steady-state conditions:

$$I_{STE} = \frac{1}{\tau_0}\int_0^d n(x)\,dx \tag{3}$$

where $n(x)$ is proportional to the effective lifetime $\tau$ of the excitons and, in addition to the exciton diffusion constant $D$ and the absorption coefficient $\mu$, $n(x)$ will be determined by the boundary conditions on the substrate ($x = d$) and the Kr/Ar interface ($x = 0$). Unfortunately these boundary conditions are controversial. Mainly two extreme cases[8] with boundary condition 1 (bc1)

$$n(0) = 0 \text{ and } n(d) = 0 \tag{4}$$

or boundary condition 2 (bc2)

$$\frac{dn}{dx}|_{x=0} = 0 \text{ and } n(d) = 0 \tag{5}$$

but also an intermediate case (bc3)

$$-D\frac{dn}{dx}|_{x=0} = -n(0)s \text{ and } D\frac{dn}{dx}|_{x=d} = -n(d)s^* \tag{6}$$

where finite surface recombination velocities $s$ and $s$* were employed. To ease the discussion we will use throughout the condition $n(d) = 0$ corresponding to $s^* \rightarrow \infty$ in accordance with the previous investigations. In ref 8 it was proven that a layer of residual gas completely quenches the exciton density. The quenching by the $MgF_2$ substrate with the mentioned presumably accumulated residual gas from the cooling cycles justifies therefore this assumption for $x = d$.

The measured thickness dependence of $I_{STE}(d)$ in Figure 1a can be fitted for bc1 and bc2 quite well with the only free parameter $l$ by taking $\mu$ from ref 21. The decay of the substrate emission due to the increasing absorption in the Kr film is consistent with the $\mu$ value as demonstrated in the inset. Fits to the decay yield $\mu$ values of 0.21 and 0.28 $nm^{-1}$ for curves 3 and 4, respectively, in accordance with 0.25 $nm^{-1}$ from ref 21. Exciton diffusion lengths $l_{min}$ of 10 and 12 nm are obtained for bc1 and bc2, respectively, which are in good agreement with the literature data $l_{min} = 10$ nm.[7] It should be emphasized that the delayed onset in the $I_{STE}$ emission compared to the decay of the substrate emission can be attributed only to $l$ values considerably exceeding the penetration depth $l_0$ of the photons. bc1 yields systematically smaller $l$ values than bc2 because the quenching ranges in the exciton densities at the outer and inner interface add up for bc1, while bc2 creates only a single quenching range at the inner interface. This behavior is demonstrated by the two $n(x)$ distributions (curves 2 and 3) for a thickness $d = 38$ nm in Figure 1b.

**TABLE 1: Exciton Diffusion Length in $n = 1$ Exciton $l_{min}$ (in nm) and Slope of Energy Dependence $\Delta l$ (in nm/eV, eq 7) from Fits of $Kr_2$* (Figure 3c) and $Kr_2F$ (Figure 3b) Intensities with Boundary Conditions bc1 (eq 4) and bc2 (eq 5)**

| | | $l_{min}$ | $\Delta l$ |
|---|---|---|---|
| $Kr_2$* | bc1 | 10.5 | 25 |
| | bc2 | 11.8 | 50 |
| $Kr_2F$ | bc1 | 10.5 | 13 |
| | bc2 | 11.8 | 32 |

The results for the fits of the thickness dependences in Figure 1a are identical for the two boundary conditions, and $I_{STE}$ versus $d_{Ar}$ cannot be used for a discrimination. The spectral dependence in Figure 3 contains more information because it covers a large spectrum of absorption coefficients $\mu$(E). The reflectivity correction via the factor $(1 - R)$ for the photon flux penetrating into the Kr film varies by 50% just in the center of the exciton band and influences the shape considerably. The limited thickness of the Kr and $F_2$/Ar layers could cause variations by interference effects, and the Ar coverage changes the step in the index of refraction. On the other hand, the absorption in the center of the exciton is so strong that it determines mainly the reflectivity, and the thickness is sufficiently large that interference effects from backside reflections are suppressed. Therefore, we refrain from calculating the multilayer reflectivity for the correction and we use the measured reflectivity.[21] In this way we avoid errors from the limited accuracy of the optical constants. The $F_2$ molecule and the F atom absorption in the Ar film is weak and structureless in this region[28,29] and therefore both species can be ignored. The intensities in Figure 3a for energies with the same $\mu$ in the $n = 1$ and $n' = 1$ bands indicate clearly that the exciton diffusion length $l$ increases with energy. Here, $l$ scales with $D$ and $\tau$ according to $l = \sqrt{D\tau}$. Relaxation within the free exciton bands and between the different free exciton branches is expected to prolong the lifetime $\tau$ before self-trapping, and $D$ may also be larger for higher exciton states. Indeed, a monotonic increase of $l$ with the exciton energy was observed in ref 9 and discussed in this spirit. We adopt the empirical description in eq 7, and we keep the diffusion length for the $n = 1$ band fixed at the $l_{min}$ values determined in Figure 1a. To higher energies beyond 10.5 eV we use the following expression (which increases linearly with $E$ (eV)):

$$l = l_{min} + \Delta l \cdot (E - 10.5) \tag{7}$$

with the slope $\Delta l$ as fitting parameter. No free parameter is left for the range of the $n = 1$ exciton except the normalization constant, and the comparison in Figure 3c shows a significantly better agreement for bc2 with the measured $Kr_2$* excitation spectrum than with bc1. The same holds also for the higher energy range for which a value of $\Delta l = 50$ nm/eV for bc2 and of 25 nm/eV for bc1 is obtained. The $l_{min}$ and $\Delta l$ values are collected in Table 1. The agreement for both boundary conditions is the worst in the minima between the excitons, and the calculated values are too large. This arises mainly from a too large absorption coefficient derived by the Kramers−Kronig analysis in ref 21 which was also observed in ref 7 and in stimulated emission experiments.[30] The dip in the center of the exciton results from the reflectivity correction with the bulk value.

A further test arises from the energy transfer and the $Kr_2F$ spectrum. bc2 (eq 5) corresponds to $s = 0$ of bc3, which means that the exciton flux to the surfaces is compensated with unity

probability by the reflected flux away from the surface. Thus, $dn/dx|_{x=0} = 0$ (as in Figure 1b curve 2), and the transfer efficiency is proportional to the exciton density $n(0)$ at the surface. For bc1 the transfer efficiency is determined by the flux of excitons to the surface $D dn/dx|_{x=0}$ and the competition of the intrinsic surface recombination velocity $s_0$ with the transfer velocity $s_F$, leading to the new effective recombination velocity

$$s = s_0 + s_F \tag{8}$$

in eq 6. The comparison of $n(0)$ calculated with bc2 and of $dn/dx|_{x=0}$ with bc1 in Figure 3b does not favor one of the boundary conditions. The $\Delta l$ values of 13 nm/eV and 32 nm/eV for bc1 and bc2 respectively are in reasonable agreement with those from the $Kr_2$* intensity according to Table 1. The general trend agrees with ref 7, and the $\Delta l$ values found here are on the lower bound of ref 7 which arises mainly from the preparation temperatures. Of course, bc1 and bc2 are only the extreme approximations for the real situation described by bc3. If $s = 0$ holds for bc2 and the uncovered Kr surface, it would be modified by the inclusion of the $F_2$/Ar top layer to a finite $s_F$ transfer rate and a finite gradient $dn/dx|_{x=0}$. In the bc1 case, $s$ would be large but finite and $n(0)$ would be very small for the clean Kr film. With F atoms, $s$ would be increased by adding $s_F$ and $n(0)$ would be further reduced. Figure 2 shows that the $Kr_2$* intensity, which monitors $\int n(x)\,dx$, decreases by 5% during exposure to the residual gas and for the coverage with $F_2$/Ar including now the energy transfer to F and $F_2$. Thus, the overall change in $n(x)$ by energy transfer is marginal, which justifies its neglect in the modeling. The comparison in Figure 3c is in clear favor of bc2 which is in agreement with ref 8 but at odds with ref 7. The continuous transition from bc2 to bc1 was demonstrated in ref 8 by accumulation of residual gas. This behavior would be hard to understand if $n(0) = 0$ (bc1) would hold already by an intrinsic $s_0 \rightarrow \infty$. Previously the intrinsic processes determining $s$ were not revealed. An enhanced self-trapping rate compared to the bulk leading to desorption,[19] a conversion of bulk excitons to surface excitons, and a decay by surface charging[31] are obvious contributions besides the extrinsic energy transfer to dopands or impurities. The three intrinsic processes (if present) would be significantly weakened in our samples by the protective covering with the Ar top layer. The $Kr_2$* intensity in Figure 2 does not change very much in going from region I to the covered region III, which is again more in favor of bc2 and a small intrinsic $s_0$.

With these considerations we have shown that the exciton distribution is well characterized with bc2 for the clean and the $F_2$/Ar covered Kr surface, and the energy transfer efficiency is proportional to $n(0)$. The modeling is based on a location of the F atoms at the Kr/Ar interface. In ref 18 a spectral shift of the emission band for $Kr_2F$ centers situated in the Kr film, at the Kr/Ar interface, or in the Ar layer was demonstrated. It was shown that the F atoms are stopped at the interface and do not penetrate from the Ar layer into the Kr film, in accordance with the presumption. Since bc2 is valid, only a smooth variation of the exciton density occurs near the interface according to curve 4 in Figure 1b. Therefore, the results of the modeling would not change even if the F atoms penetrated distances of the order of 5 nm. Now several recipes for optimal transfer and its calibration with $\int n(x)\,dx$ can be derived. The excitation intensity $I_F$ of an atom in the interface follows for the general boundary condition (bc3, eq 6) from

$$I_F = n(0)s_F \tag{9}$$

with $s_F$ according to eq 8. Therefore, $n(0)$ has to be optimized, and a thickness $d > 1/\mu$ and $d > l_0$ has to be chosen to suppress quenching effects from the backside (see Figure 1). In the case of infinite Kr layer, thickness $n(0)$ is given by[8,32]

$$n(0) = \frac{I_0(1-R)\mu\tau}{\mu l + 1}\,\frac{1}{1 + s\tau/l} \tag{10}$$

with the photon flux $I_0$. This expression can be decomposed into three factors: $I_0(1-R)$, $A = \mu l/(\mu l + 1)$, and $B = (\tau/l)/(1 + s\tau/l)$, and all have to be kept large. From B it is clear that indeed bc2 with the intrinsic $s_0 \rightarrow 0$ is optimal, and $I_F$ is given in this case by

$$I_F = I_0\,(1-R)\frac{\mu l}{\mu l + 1}\,\frac{s_F\tau/l}{1 + s_F\tau/l} \tag{11}$$

Thus, a range of $s_F\tau/l$ values of the order of $10^{-4}$ to some $10^{-1}$ is desirable to keep the $I_F$ intensity high and to provide a linear increase of $I_F$ with $s_F$ and thus with the concentration of atoms at the interface. This is just the range employed in the Kr with $F_2$/Ar studies.[18] For higher concentrations, the saturation of the signal (factor B) has to be kept in mind. The sensitivity is determined by properties of the exciton and increases with its lifetime $\tau$ and decreases with the diffusion length $l$. Of course high $s_F$ values are also relevant. According to the energetics, the Kr excitons populate efficiently the Kr*F states which relax to $Kr^+F^-$ and finally to the $Kr_2^+F^-$ state which emits.[29,33]

To optimize term A it is relevant to achieve a large product $\mu l$. Since a large $l$ value reduces the sensitivity in the B term, it is essential to keep $\mu$ as large as possible, and, concerning $l$, the balance between A and B is important. Figure 2 serves as an illustration. $I_{STE}$ of $Kr_2$* or $\int n(x)\,dx$ (eq 3) is reduced by about 5% with the addition of F and residual gas. In the center of the $n = 1$ exciton, this results in a change of $n(x)$ from curve 2 in Figure 1b to curve 4, and $n(0)$ decreases by about 7%. Term B is near 0.1 and remains reasonably well in the linear regime, and term A amounts to 0.7. Both are not far from the limit of unity and are rather optimal. The total amount of $F_2$ molecules in the $F_2$/Ar layer corresponds to 1/20 of a monolayer, and only 1/10 of them reaches the interface according to Figure 5 and ref 18. Thus, it was possible to funnel 5% of the available incoming photon flux into only about 1/200 of a monolayer of F atoms via this efficient exciton energy transfer. The signal from a direct excitation of F atoms by light corresponds to the background at energies below the $n = 1$ exciton in curve 1 of Figure 3a and is only about 1% of the signal in the exciton. Thus, the enhancement and sensitivity estimated from the measured photon fluxes in ref 18 are fully consistent with this quantitative evaluation and modeling. If one could freely choose the optimal parameters one would reduce $l$ by about a factor of 3 to increase furthermore the efficiency in term B, but term A goes down from 0.7 to 0.5 and the advantage would be only moderate.

Finally, we consider the robustness of the method concerning changes in $l$ and $\tau$ due to uncontrolled variations in preparation conditions. $I_{STE}$ (eq 3) and $I_F$ (eqs 9, 10) scale in the same way with the effective lifetime $\tau$, which includes also quenching by impurities (eq 2). Therefore, an unintentional variation in this contribution modulates $n(x)$, $I_{STE}$, and $I_F$ in the same way. Variations in $I_{STE}$ in similarly prepared samples were observed, and in fact the scaling of $I_F$ by $I_{STE}$ reduces the scatter from sample to sample considerably. This is demonstrated by the much smoother variation of the crosses in Figure 5a with spacer

layer thickness compared to the circles. Obviously this scaling enhances the robustness significantly.

Variations of the pure self-trapping lifetime $\tau_0$ with sample morphology are well documented in the literature.[34] If no quenchers at all are present in the exciton containing film (if bc2 holds) and if the radiative decay of free excitons is long compared to $\tau_0$, then $\tau = \tau_0$ and $I_{STE}$ is independent of $\tau_0$ (eqs 2 and 3). $I_F$, on the other hand, will be essentially proportional to $\tau_0$ (eqs 9, 10), and in this case the scaling of $I_F$ with $I_{STE}$ would not improve the robustness. The better statistics in Figure 5 with scaling illustrates that the varying contribution by unintentional, competing quenchers dominates the scatter of the $I_F$ values for our preparation conditions.

The linear regression in the logarithmic representation of Figure 5b yields a penetration depth of F atoms of 2.5 nm or 9 monolayers, which is consistent with the results in ref 18. The intensity at $d_{Ar} = 0$ lies above this regression. The deviation can be attributed to the $F_2$ contribution which decays with irradiation as is evident from region IV in Figure 2. A further discussion is postponed to ref 35 since there a more systematic investigation of the temperature and energy dependence together with a change from Ar to Ne films will be presented.

## Conclusion

The enhancement of the sensitivity for the detection of atoms at interfaces by exciton energy transfer can be quantitatively described by an exciton diffusion model. It is shown that a considerable amount of the incoming photon flux of the order of 10% can be funneled to coverages of only about 1/100 of a monolayer. In this way the sensitivity is increased by several orders of magnitude compared to direct light absorption. The sensitivity can be maximized by a very high absorption coefficient and a well balanced diffusion length which should not exceed the light penetration depth too much. The analytical expressions for the transfer efficiency characterize also the linear range for the detection probability. Experimental information on the integrated exciton density in the sample can be used to scale the transfer efficiency with respect to unintentional competing processes. The boundary condition with respect to the intrinsic quenching of the excitons on the interface is decisive for the sensitivity. For Kr, the determined boundary condition of essentially unity exciton reflection is favorable for the sensitivity. It is demonstrated that the Kr system is operated close to the optimal value in the experiments for F atom penetration.

**Acknowledgment.** This work was financially supported by the DFG.

## References and Notes

(1) Fugol, I. Ya. *Adv. Phys.* **1978**, *27*, 1.

(2) Schwentner, N.; Koch, E. E.; Jortner, J. *Electronic Excitations in Condensed Rare Gases*, Springer: Berlin, 1985; Chapter 6.

(3) Zimmerer, G.; Grassano, U. M.; Terzi, N., Eds. *Excited State Spectroscopy in Solids*; North-Holland: Amsterdam, 1987; p 37.

(4) Ratner, A. M. *Phys. Reports* **1996**, *269*, 197. Ratner, A. M. *J. Luminesc.* **1999**, *81*, 271. Fugol, I. Ya. *Pure Appl. Chem.* **1997**, *69*, 1219. Song, K. S.; Fu, C. R. *J. Low Temp. Phys.* **1998**, *111*, 645.

(5) Runne, M.; Zimmerer, G. *Nucl. Instr. Methods Phys. Res. B* **1995**, *101*, 156. Runne, M.; Zimmerer, G. *Nucl. Instr. Methods Phys. Res. B* **1996**, *116*, 53.

(6) Zimmerer, G. *J. Low Temp. Phys.* **1998**, *111*, 629. Kassühlke, B.; Romberg, R.; Verkamp, P.; Feulner, P. *Low Temp. Phys.* **1998**, *111*, 723.

(7) Herkert, B.; Schrimpf, A.; Göttsche, K.; Bornemann, T.; Stöckmann, H.-J. *Phys. Rev. B* **1995**, *51*, 15763.

(8) Ackermann, Ch.; Brodmann, R.; Hahn, U.; Suzuki, A.; Zimmerer, G. *Phys. Status Solidi B* **1976**, *74*, 579.

(9) Schwentner, N.; Martens, G.; Rudolf, H. W. *Phys. Status Solidi B* **1981**, *106*, 183.

(10) Jacox, M. E. *J. Mol. Spectrosc.* **1980**, *80*, 257.

(11) Jacox, M. E. *Chem. Phys.* **1979**, *42*, 113. Jacox, M. E. *Chem. Phys.* **1981**, *59*, 199.

(12) Jacox, M. E. *J. Phys. Chem.* **1983**, *87*, 4940.

(13) Jacox, M. E. *Rev. Chem. Intermed.* **1985**, *6*, 77.

(14) Sack, N. J.; Akbulut, M.; Madey, T. E.; Klein, P.; Urbassek, H. M.; Vicanek, M. *Phys. Rev.* **1996**, *54*, 5130.

(15) Haas, Y.; Samuni, U. *Prog. React. Kinet.* **1998**, *23*, 211.

(16) Apkarian, V. A.; Schwentner, N. *Chem. Rev.* **1999**, *99*, 1481.

(17) Bressler, C.; Schwentner, N. *Phys. Rev. Lett.* **1996**, *22*, 648.

(18) Bressler, C.; Dickgiesser, M.; Schwentner, N. *J. Chem. Phys.* **1997**, *107*, 10268.

(19) Kloiber, T.; Zimmerer, G. *Phys. Scr.* **1990**, *41*, 962. Hudel, E.; Steinacker, E.; Feulner, P. *Phys. Res. B* **1991**, *44*, 8972.

(20) Bahrdt, J.; Gürtler, P.; Schwentner, N. *J. Chem. Phys.* **1987**, *86*, 6108.

(21) Steinberger, I. T.; Maaskant, P.; Webber, S. E. *J. Chem. Phys.* **1977**, *66*, 4722.

(22) Belov, A. G.; Fugol, I. Ya.; Yurtaeva, E. M. *Low Temp. Phys.* **1998**, *24*, 440. Yurtaeva, E. M.; Fugol, I. Ya.; Belov, A. G. *Sov. J. Low Temp. Phys.* **1990**, *16*, 54.

(23) Gudipati, M. S.; Kalb, M. *Chem. Phys. Lett.* **1999**, *307*, 27.

(24) Goodman, J.; Brus, L. E. *J. Chem. Phys.* **1977**, *67*, 4858.

(25) Schriever, R.; Chergui, M.; Kunz, H.; Stepanenko, V.; Schwentner, N. *Chem. Phys.* **1989**, *91*, 4128.

(26) Kuszner, D.; Schwentner, N. *J. Chem. Phys.* **1993**, *98*, 6965.

(27) Danilychev, A. V.; Apkarian, V. A. *J. Chem. Phys.* **1993**, *99*, 8617. Danilychev, A. V.; Apkarian, V. A. *J. Chem. Phys.* **1994**, *100*, 5556.

(28) Bressler, C.; Lawrence, W.; Schwentner, N. *J. Chem. Phys.* **1996**, *105*, 1318.

(29) Bressler, C.; Lawrence, W.; Schwentner, N. *J. Chem. Phys.* **1996**, *105*, 10178.

(30) Schilling, G.; Ernst, W. E.; Schwentner, N. *IEEE J. Quantum Electron.* **1993**, *29*, 2702.

(31) Kraft, J.; Schrimpf, A.; Schweitzer, B.; Ibbeken, K.; Stöckmann, H. J. *Europhys. Lett.* **1997**, *39*, 459.

(32) DeVore, H. B. *Phys. Rev.* **1956**, *102*, 86.

(33) Bressler, C.; Lawrence, W.; Schwentner, N. *J. Chem. Phys.* **1995**, *102*, 48.

(34) Varding, D.; Reimand, I.; Zimmerer, G. *Phys. Status Solidi B* **1994**, *185*, 301. Varding, D.; Becker, J.; Frankenstein, L.; Peters, B.; Runne, M.; Schröder, A.; Zimmerer, G. *Low Temp. Phys.* **1993**, *19*, 427.

(35) Dickgiesser, M.; Schwentner, N., to be published.